Macromolecules

pubs.acs.org/Macromolecules Article

Polyelectrolyte Complex Coacervation across a Broad Range of Charge Densities

Angelika E. Neitzel, Yan N. Fang, Boyuan Yu, Artem M. Rumyantsev, Juan J. de Pablo,* and Matthew V. Tirrell*

Cite This: *Macromolecules* 2021, 54, 6878−6890 Read Online

ACCESS | Metrics & More | Article Recommendations | Supporting Information

ABSTRACT: Polyelectrolyte complex coacervates of homologous (co)polyelectrolytes with a near-ideally random distribution of a charged and neutral ethylene oxide comonomer were synthesized. The unique platform provided by these building blocks enabled an investigation of the phase behavior across charge fractions $0.10 \leq f \leq 1.0$. Experimental phase diagrams for $f = 0.30-1.0$ were obtained from thermogravimetric analysis of complex and supernatant phases and contrasted with molecular dynamics simulations and theoretical scaling laws. At intermediate to high f, a dependence of polymer weight fraction in the salt-free coacervate phase ($w_{P,c}$) of $w_{P,c} \sim f^{0.37\pm0.01}$ was extracted; this trend was in good agreement with accompanying simulation predictions. Below $f = 0.50$, $w_{P,c}$ was found to decrease more dramatically, qualitatively in line with theory and simulations predicting an exponent of 2/3 at $f \leq 0.25$. Preferential salt partitioning to either coacervate or supernatant was found to be dictated by the chemistry of the constituent (co)polyelectrolytes.

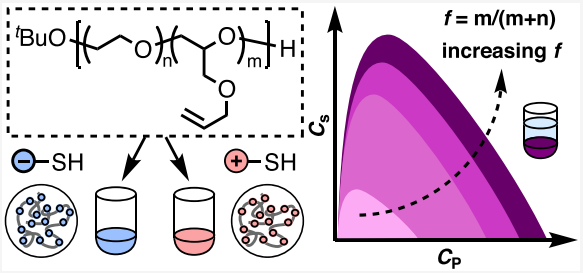

INTRODUCTION

Mixing of oppositely charged polyelectrolytes (PEs) in solution generally elicits an associative phase separation into a polymer-lean supernatant phase and a polymer-rich polyelectrolyte complex (PEC) phase.[1−4] This complexation of oppositely charged PEs produces either opaque solids—kinetically trapped glasses—or transparent, viscous liquids—usually closer to or at thermodynamic equilibrium—called polyelectrolyte complex coacervates.[5,6] In nature, PECs form the constituents of complex multicomponent membraneless organelles in cells,[7,8] play key roles in post-transcriptional processes,[9] and give rise to functional and responsive materials.[10,11] PECs are also thought by some to have a role in the origins of life.[12] From a materials' engineering perspective, they are useful candidates for therapeutic protein and nucleotide delivery.[13,14] Academic interest further encompasses their study in the context of stimuli-responsive hydrogels,[15,16] enzyme encapsulants,[17,18] membranes,[19−21] electrospun fibers,[22,23] and salt processable materials (saloplastics).[24] Each of these applications is enabled by the specific phase behavior and viscoelastic properties of a PEC under a given set of conditions. Therefore, understanding and controlling PEC phase behavior are key to enabling bottom-up, rational material design.

Properties of PECs are dictated by many factors, including molecular characteristics of the component PEs such as their degree of polymerization (N),[25−27] charge density or charge fraction (f),[28−30] blockiness of charges along the chain,[31−33] polymer hydrophilicity or polarity,[34−36] tacticity or chirality,[37] and architecture.[38] Effective chemical interaction parameters describing the interplay between all species in the system—solutes and solvents—have to be considered. This can be achieved by introducing the corresponding Flory−Huggins interaction parameters (χ_{ij}) for PE−PE, PE−solvent, and PE−salt.[34,35] For the latter case, specific ion effects—which are qualitatively predicted by the Hoffmeister series—and ion valency have to be taken into account.[39] Lastly, environmental conditions such as the solution ionic strength (I),[40] dielectric constant (ϵ),[41] pH,[42] and temperature (T)[43] can enhance or diminish the strength of pertinent non-covalent interactions. In view of this vast parameter space, it is unsurprising that the development of theoretical models capable of capturing all such effects to produce broadly applicable predictions has been challenging.

Although the process of complex coacervation was first described in 1929 by Bungenberg-de Jong and Kruyt,[44] rigorous quantifications of complex and supernatant phase compositions in the construction of binodal phase diagrams have only been reported over the past decade. Given the breadth of works examining PECs, we confine ourselves here to the discussion of a few relevant examples that have probed

Received: March 29, 2021
Revised: May 19, 2021
Published: July 6, 2021

https://doi.org/10.1021/acs.macromol.1c00703
Macromolecules 2021, 54, 6878−6890

how PE molecular characteristics impact PEC phase behavior and that have quantified macrophase compositions. In 2010, Spruijt et al. published binodal phase diagrams for PECs of poly(acrylic acid) [PAA] and poly(*N*,*N*-dimethylaminoethyl methacrylate) [PDMAEMA] with N = 20, 50, 150, and 510.[26] Fluorescein-labeled PAA concentration in the supernatant was measured via fluorescence spectroscopy and subsequently used together with macrophase volume and coacervate dry mass measurements to quantify the amount of water and PAA in each phase. Salt concentrations (C_s) were not directly measured; the authors assumed them to be equal in both phases and additive to yield the concentration of salt at which each sample was prepared ($C_{s,i}$), illustrated by phase diagrams with horizontal tie lines. Li et al. constructed binodal phase diagrams for complexes of poly(L-lysine hydrochloride) (PLK) and poly(sodium D,L-glutamate) (PRE), systematically varying N, initial PE concentration ($C_{P,i}$), and $C_{s,i}$.[27] The authors used a combination of thermogravimetric analysis (TGA), turbidity, and conductivity measurements to measure C_s and PE concentration (C_P) in supernatant and coacervate phases. Salt resistance—a measure of the highest $C_{s,i}$ at a given $C_{P,i}$ where macroscopic phase separation still takes place—was determined by a combination of optical microscopy and turbidity measurements. Collectively, these works demonstrated that (1) longer chains (i.e., higher N) afford denser complexes (i.e., higher C_P) with higher critical salt concentrations ($C_{s,cr}$), (2) coacervates prepared at a higher $C_{P,i}$ exhibit a lower resistance to dissolution with salt ("self-suppression"), and (3) the experimental phase diagrams departed from the Voorn−Overbeek theory[45] in that complexes had higher polymer density than predicted and that salt was observed to partition preferentially into the supernatant phase.

Synthetic PECs studied thus far have predominantly dealt with fully or strongly charged PEs, i.e., those where all or a majority of monomer units are ionized, respectively.[46] For this reason, the role of PE linear charge density—or the fraction of ionic monomers f—in PE complex coacervation remains almost experimentally unexplored. At the same time, theoretical studies suggest that f can be used to tune the binodals of the associative phase separation as well as the internal structure and density of the PEC phase.[47−50] A notable exception is a recent experimental investigation of PE charge fraction and polarity effects on PEC phase behavior by the Laaser group. By use of optical turbidity, it was shown that salt resistance decreased with diminishing f (down to f = 0.67) but was surprisingly insensitive to comonomer hydrophobicity in that range of charge densities.[51] In addition, the authors reported coacervate compositions measured by TGA for homologous hydrophobic and hydrophilic series (f = 0.67−1.0) prepared at 0.2 M potassium chloride (KCl). From these data, the authors concluded that phase behavior was dominated by charge density with the caveat that the hydrophobicity of the chains may have a greater impact at lower f.

The present study is aimed at the systematic comparison of complex coacervation across a broad range of PE linear charge densities. We present binodal phase diagrams for PECs with f = 0.30−1.0 where amounts of water, (co)polyelectrolyte [(co)-PE], and salt in coacervate and supernatant phases were quantified by TGA, as pioneered by Li et al.[27] To separate the role of PE charge density from other effects such as hydrophobicity[29,51] and stiffness,[30] a series of well-defined, homologous (co)PEs with precisely controlled f values and near ideally random monomer distributions were synthesized. The (co)PEs are water-soluble across all charge densities, which is in stark contrast to frequently studied hydrophobic PEs that are water-soluble only when a significant fraction of their monomers is ionized. Furthermore, polycation oxidation facilitated a critical analysis of how PE polarity and solvation ability, in addition to f, impacts salt partitioning between macrophases. This provides, to the best of our knowledge, the first quantitative understanding of C_P dependence on f for PECs across a broad range of charge densities.

EXPERIMENTAL AND SIMULATION METHODS

Polymer Synthesis and Functionalization. Poly(allyl glycidyl ether) [poly(AGE)] and poly(allyl glycidyl ether-*stat*-ethylene oxide)s [poly(AGE-*stat*-EO)s] were synthesized by using oxyanionic ring-opening copolymerization of ethylene oxide (EO) and allyl glycidyl ether (AGE) according to a previously reported procedure.[52] Polymerizations were initiated with commercial potassium *tert*-butoxide solution in tetrahydrofuran (1 M in THF)[53] to afford polymers of number-average degree of polymerization (N_n) = 200 ± 10% and containing mole fractions AGE of 0.10, 0.30, 0.54, 0.72, or 1.0 (f_{AGE}). Crude polymerization mixtures were precipitated into cold hexanes (−78 °C); the purified polymers were dried under high vacuum and stored in a −78 °C freezer. Postpolymerization modification by thiol−ene click chemistry was performed by using azobis(isobutyronitrile) (AIBN) (0.7 equiv per mole of alkene) and either cysteamine hydrochloride (20 equiv per mole of alkene) or sodium 3-mercapto-1-propanesulfonate (10 equiv per mole of alkene) in a degassed solution of 5/1 dimethylformamide (DMF)/water (H_2O) or 3/1 DMF/H_2O, respectively, at 80 °C. Upon full consumption of alkenes, the (co)PEs were purified by dialysis in snakeskin tubing (MWCO = 3.5 kg/mol, eight cycles) against 4 L of Milli-Q water (or Milli-Q water acidified to pH 3−4 for polycations), concentrated in Amicon-15 tubes [MWCO = 3 or 10 kg/mol, depending on (co)PE number-average molar mass (M_n)], filtered through 0.22 μm polyethersulfone membranes, and lyophilized. All neutral polymers were characterized by proton (^{1}H) nuclear magnetic resonance (NMR) spectroscopy to establish M_n by end-group analysis, and a size exclusion chromatograph (SEC) equipped with a refractive index detector was used to determine neutral (co)polymer dispersity ($Đ$) by using 0.01 M sodium bromide in DMF as eluent (Figures S1 and S2). Neat (co)PEs were characterized by ^{1}H and carbon (^{13}C) NMR spectroscopy (Figures S3−S6).

PEC Preparation and Salt Resistance Measurements. Purified (co)PEs were dissolved in Milli-Q water at a final concentration of 50 mg/mL, and the pH was adjusted to 3−4 with 1 M hydrogen chloride (HCl) to ensure full ionization of amines (see the Supporting Information for a discussion on the observed phase behavior when stock solutions were not acidified). Thereafter, (co)polycation solutions were treated with hydrogen peroxide (2 equiv per mole of sulfur), vortexed, and heated at 37 °C for 30 min to oxidize thioether side chains to a mixture of sulfoxide and sulfonium moieties as previously reported (Figures S7 and S8).[34] To ensure that the polyether backbone was stable to treatment with H_2O_2, we functionalized poly(AGE-*stat*-EO) with f_{AGE} = 0.54 using hexanethiol, subjected the resultant neutral copolymer to the same oxidation conditions, and characterized it by DMF SEC before and after oxidation. The SEC trace showed no shift in molar mass with oxidation (Figure S9), confirming that polyether backbones were not subject to oxidative cleavage with H_2O_2. A sample of poly(ethylene oxide) with N_n ∼ 105 was furthermore treated with H_2O_2, and ^{1}H NMR spectral analysis indicated no changes to the polymer structure with oxidation (Figure S10). To determine degree of thioether oxidation, we treated copolycations with f = 0.30 and 0.72 with 0.5−2 equiv of H_2O_2 and monitored structural changes by ^{1}H NMR spectroscopy (Figures S11 and S12). Although sulfoxide and sulfonium moieties could not be distinguished by this method, it was evident that thioether moieties were completely consumed with 2

https://doi.org/10.1021/acs.macromol.1c00703
Macromolecules 2021, 54, 6878−6890

equiv of H_2O_2. PECs were prepared with the desired final (co)PE and sodium chloride concentrations ([NaCl]) by sequential addition of acidified Milli-Q water, acidified 5 M stock solution of $NaCl_{(aq)}$ (prepared with a 100 mL volumetric flask), (co)polycation stock solution, and (co)polyanion stock solution. Samples were vortexed for 30 s, and (co)PE complex droplets were analyzed for each charge fraction across a range of exogenous [NaCl] by using phase contrast optical microscopy (Leica DMI 6000B). For each condition, 100 μL of sample solution was injected into ultralow attachment 96-well plates (Costar, Corning Inc.) for observation.

Thermogravimetric Analysis. Supernatant (20−60 mg) and complex phases (4−60 mg) were harvested for TGA to determine phase compositions. All samples were prepared in 1.5 mL scale Eppendorf tubes centrifuged for 20 min at 17000*g*, after which two transparent phases were obtained. The TGA measurement was first conducted on TA Instruments SDT 600 TGA by using aluminum pans in air. The following protocol was followed: the temperature was ramped up from room temperature to 110 °C at 8 °C/min, held at 110 °C for 90 min, ramped to 600 °C at 10 °C/min, and then held at 600 °C for 120 min. The combined weight of the pan and the sample was recorded along the heating procedure to extract the weights of water, (co)polyelectrolyte, and salt contents in each phase. A similar protocol was followed in furnace burning experiments using a Barnstead Thermolyne Furnace 1400. The samples were placed in the furnace at room temperature; the temperature of the furnace was increased to 110 °C and held there for 2.5 h. At that point, the samples were cooled to room temperature, their weights were recorded to estimate the water contents, and the samples were again placed into the furnace and heated to 600 °C. After heating for 12 h, the samples were cooled to room temperature, and their weights obtained again to estimate the co(polyelectrolyte) and salt contents. For each (co)polyelectrolyte and salt concentration, samples were prepared at least in triplicate. To verify that the residue remaining after the 12 h isotherm at 600 °C was attributable solely to NaCl and not contaminated with polymer degradation products, samples of all f values were prepared at known exogenous [NaCl] and subjected to TGA; the theoretical mass of salt in the sample was compared to the mass of the residue after the 600 °C isotherm (Table S1). Finally, to access one additional data point, endogenous NaCl (i.e., PE counterions) was washed out from coacervates prepared at 0 M exogenous NaCl by using Milli-Q water adjusted to pH ∼ 3−4. Although two wash cycles did not afford entirely salt-free coacervates—presumably due to the ions introduced by the pH-adjusted water—the coacervate salt concentrations were significantly lowered.

Simulation Model of the System. A Kremer−Grest model[54] including Coulomb interactions between monomers was used to simulate complex coacervation. Specifically, PEs are represented as chains of spherical interaction sites or beads connected by springs, and salt ions are modeled by single spheres. To reduce computational power, solvent was implicitly included as a continuum medium. All sites were of the same size, $r = \sigma$ (reduced units were used for simulation). A finitely extensible nonlinear elastic (FENE) potential was used for bonded interactions, and excluded volume (non-Coulomb) interactions were modeled by shifted and truncated Lennard-Jones (LJ) potentials. Two scenarios were considered: one in which all sites experience the same LJ interaction potential and another in which salt−monomer interactions differ from (are more attractive than) salt−salt and monomer−monomer interactions. Coulomb interactions between charged sites were calculated by a particle−particle particle-mesh method in LAMMPS.[55] The details of the interaction formulas and parameters can be found in the Supporting Information. In this work we use a Θ solvent with T_Θ = 3.18 (i.e., $\epsilon_{LJ} = 0.314 k_B T$)[56] maintained by a Langevin thermostat.

In our simulations, we use a minimal coarse-grain model with an implicit solvent that can capture the main trends in the system's behaviors. A quantitative level of description of the experimental data may be achieved by resorting to more sophisticated simulation approaches. The different polarizabilities of the PEs, the solvent, and the salt ions can all be taken into account via appropriate model parametrization,[57,58] introducing an additional ion-dipole $\sim 1/r^4$ interaction potential between the beads,[59] and by using polarizable beads comprising Drude oscillators or beads with permanent dipoles.[59,60] To fully address the microscopic specificity of all species responsible for solvation, hydrogen bonding, chirality effects, and so on, atomistic simulations should be performed.[37,61]

The charge fraction f is given by the ratio of charged over total number of monomers in the PE chain. For chains of the same f value, previous studies[31−33] have shown that the sequence of charged and neutral monomers significantly impacts phase behavior in PECs. To take this effect into account and to mimic the statistics of random coPEs, we used two methods of sequence generation that maintain the same f values. Within the first method, we generated ideally random sequences of length N = 200 by using a first-order Markov process, with the eigenvalue of the Markov transition matrix (the measure of charge blockiness) set to $\lambda = 0$.[33,62] These systems were only used to calculate the dependence of salt-free coacervate density on f and compare it with scaling predictions.[47−50] The second method was used to properly model poly(AGE-*stat*-EO)-derived coPEs synthesized by the statistical copolymerization of AGE and EO monomers with 100% conversion. The actual sequences of these coPEs deviate from the ideally random case because of a nonzero correlation parameter, $\lambda \neq 0$, and copolymer compositional drift.[63] To mimic the experimental chains, we generated sequences using the "Compositional Drift" software[64] provided with the known reactivity ratios for AGE and EO monomer and the initial feed ratios (i.e., f values) used in the corresponding experiments.[63] This program uses a Monte Carlo method to generate different realizations of sequences corresponding to the Mayo−Lewis model of copolymerization kinetics. The resulting sequences exhibited minor compositional drift for chains with N_n = 200 and $Đ$ = 1.01. These were used for the calculation of binodal curves and for comparison with experiments. As shown below, the results corresponding to these two different ways of generating sequences differ only marginally.

Isothermal−Isobaric (*NpT*) Ensemble for Salt-Free Coacervates. To simulate the salt-free coacervate phase in the equilibrium state, the simulation box was maintained in an *NpT* ensemble with p = 0 since the osmotic pressure of the polymers in highly diluted supernatant coexisting with the coacervate is close to 0.[49,65] This *NpT* ensemble was achieved by coupling a Berendsen barostat and a Langevin thermostat with damping parameter $\Gamma = 1.0m/\tau_{LJ}$, where τ_{LJ} is the reduced time unit and m = 1 is the reduced particle mass. The bead velocities and positions were updated by a velocity-Verlet algorithm. The time step was set to be $0.002\tau_{LJ}$. Equilibration was ensured by considering the decay of the end-to-end vector correlation function[49,65] and the convergence of the density as a function of time. The average density was obtained after equilibration with a block average.

Gibbs Ensemble Simulation of Phase Coexistence. With the addition of salt ions, binodal curves must be calculated by equilibrating supernatant and coacervate phases. To this end, we used a hybrid MC/MD Gibbs ensemble simulation.[66] A further simplification can be made by assuming there is no polymer in the supernatant phase, which is appropriate unless the critical salt concentration is approached.[67] Experimental binodals obtained in this and earlier studies[26,27] serve to justify this assumption and demonstrate that the density of the supernatant substantially deviates from zero and becomes comparable with that of the coacervate only in a very narrow range of salt concentrations, close to the critical point. Because our simulations are not aimed at describing the solution's critical behavior, the assumption adopted in this work, which strongly simplifies the simulation procedure, is reasonable. For the range of parameters considered here, it leads only to a minor overestimation of the coacervate density, but it does not affect the main findings about the phase behavior such as the shift of the binodals for decreasing f, salt partitioning, scaling for the salt-free coacervate density, and so on.

The coexisting phases are represented by two boxes. One contains salt beads to mimic the supernatant phase, whereas the other corresponds to the coacervate and contains salt and polymers. Phase equilibrium was achieved by randomly choosing one of three events:

https://doi.org/10.1021/acs.macromol.1c00703
Macromolecules 2021, 54, 6878−6890

(i) *NVT* MD runs within each box for relaxing the system, (ii) particle transfer moves where a pair of oppositely charged salt beads were moved from one box to another, or (iii) volume exchange moves between two boxes. The acceptance criteria for moves ii and iii can be readily derived from the classical *NVT* Gibbs ensemble method.[68] We implemented this method as Python scripts to drive the simulation in LAMMPS.[69] In this work, the combined volume of the two phases is up to $80000\sigma^3$ to ensure adequate volumes for each phase and avoid finite-size effects. The total number of coPE chains in the coacervate phase is fixed to 60. The initial configuration of the coacervate phase was generated through a self-avoiding random walk. For the same initial average concentration of polymer and salt, we conducted two independent runs, where the initially assigned volumes for supernatant and coacervate phases were different. Namely, one run had a dense coacervate phase at the beginning while the other started with the polymer-containing phase of large volume and hence low density. These two systems were shown to converge to similar points along the binodal curves, serving to underscore the validity of our procedures.

EXPERIMENTAL RESULTS

(Co)PE Synthesis and PEC Preparation. The monomers employed in the synthesis of the (co)PEs reported here were specifically chosen to isolate the effects of charge density on polyelectrolyte complex coacervate phase behavior systematically across a broad range of charge densities. This required meeting specific design parameters including (1) choosing a neutral, hydrophilic comonomer that would afford water-soluble copolyelectrolytes even at low f values, (2) identifying a comonomer pair that polymerizes randomly to avoid blocky charged regions, (3) producing long enough chains such that coacervation still occurs at low f, (4) using polyanion/polycation pairs that are perfectly matched in N_n, f, and $Đ$, (5) reducing as well as possible other non-covalent interactions, such as hydrophobic, cation−π and/or $\pi-\pi$ interactions, and hydrogen bonding between monomers, and (6) identifying a system that afforded homogeneous liquid coacervates—i.e., true equilibrium structures—across the entire spectrum of exogenous salt concentrations.

As poly(ethylene oxide) (PEO) and strongly charged polyelectrolytes are water-soluble at ambient conditions, we predicted that water solubility would be enabled by abundant ionic groups at high f values whereas increasing relative amounts of EO would promote solubility at low f values [for PEO: solubility parameter δ = 9.9 $(\text{cal/cm}^3)^{1/2}$)].[70] The reactivity ratios of solution EO/AGE copolymerization in tetrahydrofuran (THF) at 45 °C have been previously established by Lynd and co-workers as r_{AGE} = 1.31 ± 0.26 and r_{EO} = 0.54 ± 0.03; hence, a near-random distribution of monomers along the chain is anticipated.[52] Compositional drift becomes significant at high monomer conversions for this system, and we note that for the copolymers reported here polymerizations were not quenched prior to reaching 100% conversion. We have therefore generated sequences corresponding to the experimental reactivity ratios and feed ratio f using a recently published Compositional Drift program[63,64] and have provided MD simulation results that take into account length and sequence polydispersities and compositional drift.

Well-defined (co)polymers with $N_n \sim 200$ were obtained by the oxyanionic (co)polymerization of EO and AGE with f_{AGE} = 0.10, 0.30, 0.54, 0.72, and 1.0 (Table 1 and Figure S2). Reaction times were carefully adjusted to minimize isomerization of AGE to the internal cis olefin for all copolymers; all of the polymers reported here contained <7% of isomerized AGE units (cf. Figure S1).[71] Isomerization was observed to increase significantly—even at 45 °C—if the polymerization was not terminated once full conversion was achieved. A systematic comparison of coacervates formed with chains containing a high fraction of isomerized alkenes was not carried out, as such an endeavor is outside of the scope of this work. However, one may speculate that the chemical environment adjacent to the thioether becomes more hydrophobic and sterically encumbered with alkene isomerization, which would be expected to produce slight differences in the phase behavior of complexes formed from chains with a high degree of alkene isomerization. Homologous (co)polycation/(co)polyanion pairs were accessed by postpolymerization modification of neutral (co)polymers using thiol−ene click chemistry (Scheme 1). Here it is important to note that even small residual amounts of unfunctionalized alkenes (∼1−5%) resulted in the formation of cross-links during lyophilization, evidenced by PE gelation upon attempted redissolution in water. Therefore, complete conversion of alkenes was carefully verified for all of our samples.

Table 1. Molecular Characteristics of Precursors to Homologous Polyanion/Polycation Pairs

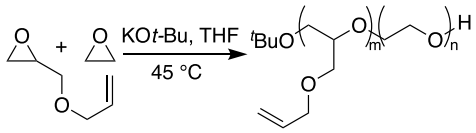

sample name	M_n [a] (kg/mol)	N_n [a]	f_{AGE} [a]	$Đ$ [b]
poly(AGE_{19}-*stat*-EO_{168})	10	187	0.10	1.12
poly(AGE_{55}-*stat*-EO_{128})	12	183	0.30	1.16
poly(AGE_{113}-*stat*-EO_{96})	17	209	0.54	1.20
poly(AGE_{151}-*stat*-EO_{60})	20	211	0.72	1.17
poly(AGE_{209})	24	209	1.0	1.18

[a]Determined from ^{1}H NMR spectroscopy. [b]Measured by DMF SEC with a refractive index detector.

(Co)polyanions [poly(Sulf-*stat*-EO), Scheme 1] displayed excellent solubility across the entire range of f values in water and a broad range of [NaCl] (Figure S14). For (co)polycations, we first examined pH-independent guanidinium-functionalized (co)polycations [poly(Guan-*stat*-EO), Scheme 1] and found them to exhibit poor solubility in aqueous NaCl (Figure S4). This was observed most dramatically for high f values, revealing the hydrophobic nature of the guanidinium-functionalized AGE monomer upon the screening of charges with exogenous salt.[72,73] Polyelectrolyte complexes prepared from poly(Guan)/poly(Sulf) could not be dissociated with NaCl as poly(Guan) itself became visibly insoluble at [NaCl] ∼ 0.4 M (Figure S13). We did however find that poly(Guan) remained soluble in monobasic sodium phosphate (NaH_2PO_4) solutions and that the corresponding complexes could be dissociated at [NaH_2PO_4] ∼ 4 M (Figure S14). This suggests that the guanidinium chloride ion pair is not solvated as well as the corresponding guanidinium sodium dihydrogen phosphate ion pair. As NaH_2PO_4 is not thermally stable above 169 °C, we changed the ion identity of the (co)polycation from guanidinium to ammonium to promote complex dissolution with NaCl to simplify the analysis of TGA experiments. We reasoned that guanidine has a lower water solubility than ammonia; hence, ammonium-functionalized AGE monomers are expected to remain soluble to a higher [NaCl] than guanidinium-functionalized AGE monomers. Indeed, the

https://doi.org/10.1021/acs.macromol.1c00703
Macromolecules 2021, 54, 6878−6890

Scheme 1. Synthesis of Homologous, Statistical Copolyanions and Copolycations with $f = m/(m + n)$ [$m = o + p$ for Oxidized (Co)polycations and $n = 0$ for Fully Charged Polyelectrolytes]

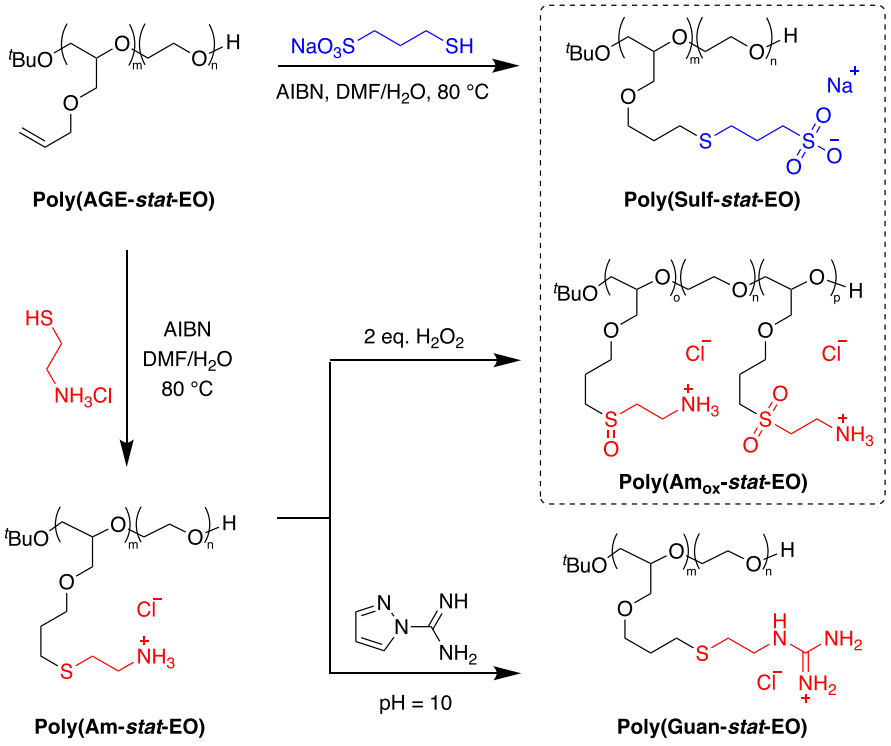

analogous poly(Am) (Scheme 1) was fully soluble up to [NaCl] = 4 M (Figure S13). Nevertheless, complex coacervates of poly(Am)/poly(Sulf) could not be dissociated with the experimentally highest accessible exogenous [NaCl] of 4 M (*vide infra*).

Rather than screening other salts for the dissociation of our complexes, we instead further assimilated (co)polycation and (co)polyanion polarities via oxidation of (co)polycation thioether side chains with hydrogen peroxide (H_2O_2); this was inspired by a recent disclosure by Xia and co-workers.[34] Oxidation with 2 equiv of H_2O_2 to thioether moieties afforded (co)polycations with a mixture of sulfoxide and sulfonium side chains [poly(Am_{ox}-*stat*-EO), Scheme 1] that were soluble across a broad range of [NaCl] at all f values (Figure S13). On the basis of previous model studies,[34] we estimated that sulfoxide (subscript o) and sulfonium (subscript p) moieties were present in an ∼1:1 ratio after oxidation with 2 equiv of H_2O_2 (i.e., $o \sim p$ and $m = o + p$; Scheme 1).

Effect of Polycation Thioether Oxidation on Phase Behavior. Polyelectrolyte complex coacervates were prepared for TGA from fully charged (i.e., $f = 1.0$) poly(Am)/poly(Sulf) and poly(Am_{ox})/poly(Sulf). The complex and supernatant compositions are displayed in a salt concentration [C_s (wt %)]−polyelectrolyte concentration [C_P (wt %)] plot in Figure 1. Without oxidation of polycation thioether moieties, poly(Am)/poly(Sulf), prepared at 0 M exogenous NaCl, contained 46 wt % polyelectrolyte. The density of the complex phase (C_P) was observed to decrease up to [NaCl] = 2 M; thereafter, it remained roughly constant around $C_P \sim 30$ wt % up to [NaCl] = 3 M (Table S2). Between [NaCl] = 3 and 4 M, an increase in coacervate density was observed. This behavior is well in line with that for previously described PECs stabilized by non-covalent interactions other than electrostatics.[35,74] In comparison, the analogous coacervate formed with poly-

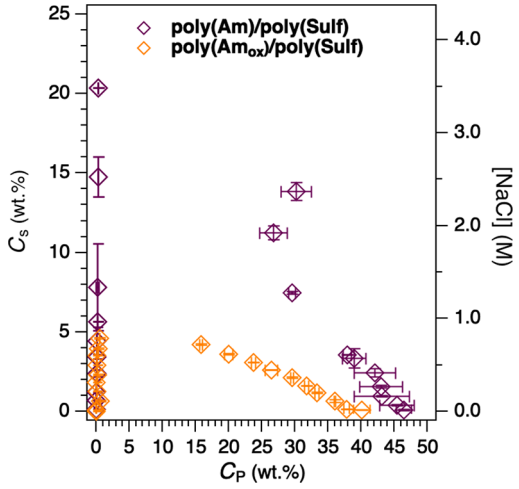

Figure 1. Binodal phase diagrams for PECs prepared from polycations used as synthesized [poly(Am)] vs oxidized with 2 equiv of H_2O_2 relative to thioether moieties [poly(Am_{ox})]. All samples were prepared with $C_{P,i}$ = 1 wt %, and error bars present standard deviations between measurements performed in triplicate.

(Am_{ox})/poly(Sulf) was characterized by a lower coacervate density, with $C_P \sim 37$ wt % that diminished with increasing [NaCl] and was fully dissolved at [NaCl] = 1.0 M (Table S3). The narrowing of the binodal phase envelope and decrease of $C_{s,cr}$ with polycation oxidation are consistent with observations by Lou et al.[34] for PECs that were not otherwise stabilized by nonelectrostatic interactions. We concluded from these data that polycation thioether oxidation was effective in modulating the polarity of the ammonium-functionalized AGE monomer to enable a systematic comparison of coacervate properties as a

https://doi.org/10.1021/acs.macromol.1c00703
Macromolecules 2021, 54, 6878−6890

function of electrostatics without significant confounding hydrophobic interactions.

Effect of *f* on Phase Behavior. Phase morphology and salt resistance of PECs prepared from homologous poly(Sulf-*stat*-EO) and poly(Am_{ox}-*stat*-EO) were first qualitatively examined by bright field optical microscopy (Figure 2). No

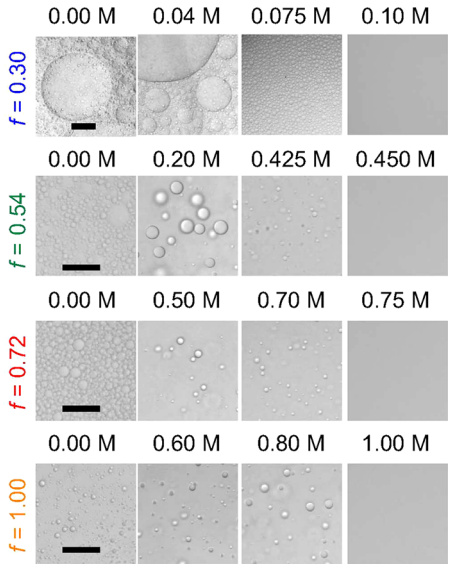

Figure 2. Bright field optical microscopy images obtained across indicated charge fractions and sodium chloride salt concentrations. Polymer concentrations were 10 mg/mL for all *f* values, and samples were analyzed immediately after complexation. Top row scale bar: 250 μm; second to fourth row scale bars: 50 μm.

macroscopic phase separation was observed for complexes of f = 0.10. Colloidal coacervate suspensions obtained for f = 0.30−1.0 were transferred to well plates immediately after preparation and imaged. Formation of liquid complexes was evidenced by spherical droplets observed under the microscope. As expected, complexes of higher charge densities exhibited increased resistance to dissolution with NaCl.

Informed by salt resistance measurements, PECs were prepared for TGA from poly(Am_{ox}-*stat*-EO)/poly(Sulf-*stat*-EO) with f = 0.30−1.0 to elucidate the effect of linear charge density on the PEC phase behavior. Samples containing coacervate droplets were centrifuged to yield two macroscopically phase-separated, transparent liquid phases, indicative of equilibrium structures devoid of inhomogeneities that cause light scattering (Figure 3). Coacervate volume was observed to

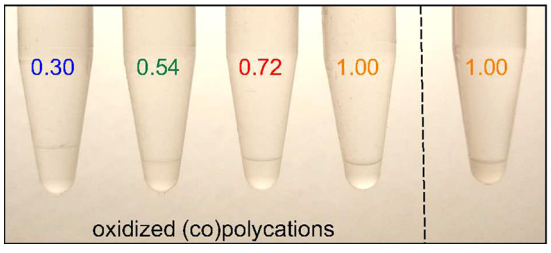

Figure 3. Macroscopically phase-separated samples obtained after centrifugation from oxidized polyelectrolytes with f = 0.30−1.0 (left) and fully charged coacervate obtained without polycation oxidation (right). All samples are at equilibrium as indicated by the presence of two transparent liquid phases.

increase with decreasing PE linear charge density; this trend is expected as decreasing f is similar to doping a fully charged complex with salt.

Coacervate Density at 0 M Exogenous Salt Varies Only Marginally for $f \geq 0.5$. Supernatant and coacervate phases were harvested to determine their water, (co)PE, and salt weight fractions for samples doped with a range of [NaCl]. As expected, $C_{P,i}$ determined PEC salt resistance but did not impact the ultimate shape of the binodal phase diagram and the PEC critical salt concentration ($C_{s,cr}$). A C_P of 1 wt % (= 10 mg/mL) was chosen as this broadened the range of accessible [NaCl] compared with complexes prepared at higher $C_{P,i}$, thereby simplifying the experimental procedure and reducing error in the analysis. Binodal phase diagrams for PECs with f = 0.30−1.0 (Figure 4, Figures S15 and S16, Tables S3−S6) are

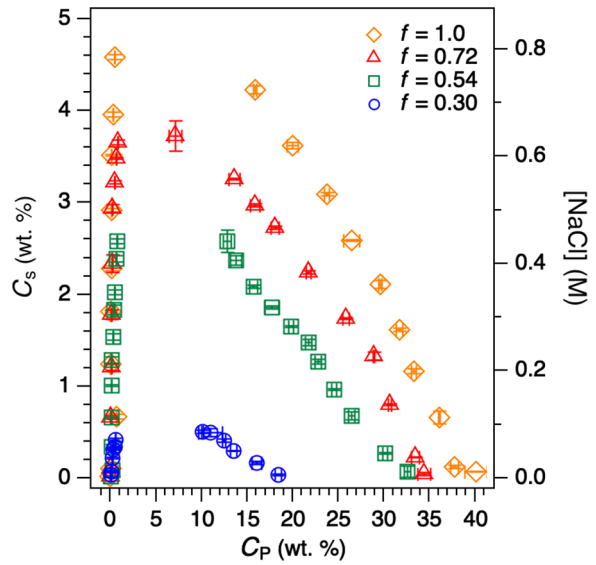

Figure 4. Experimental binodal phase diagrams for PECs with f = 0.30−1.0 and $C_{P,i}$ = 10 mg/mL obtained from TGA. The highest C_P values correspond to samples prepared at 0 M exogenous [NaCl] and washed twice with acidified water to reduce coacervate salt content. All measurements were performed in triplicate, and error bars represent the standard deviation between samples.

qualitatively in line with expectations: the two-phase envelope narrows, and $C_{s,cr}$ diminishes with decreasing f. Across the f values presented here, the majority of the (co)PEs are localized in the complex phase with (co)PE content in the supernatant phases increasing up to 0.5 wt % at the highest [NaCl]. Coacervate density *in the absence of exogenous salt* (not to be confused with coacervates obtained after salt-washing experiments removing *endogenous (co)PE counterions*) decreased only marginally when cutting the PE charge density into half, from C_P = 38 wt % for f = 1.0 to C_P = 29 wt % for f = 0.54. These results indicate a weak dependence of coacervate density on f within a regime of high charge density (f = 0.54−1.0). A pronounced decrease in coacervate density is, however, observed for the analogous case of f = 0.30, with C_P = 16 wt %, down from C_P = 29 wt % at f = 0.54.

Effect of *f* and PE Chemistry on Salt Partitioning. An interesting feature of the PECs described here is the observed salt partitioning between the complex and supernatant phases. Tie lines have been added to the binodal phase diagram for f = 0.54 (Figure 5A). It can be seen that the tie lines have a positive slope at low to intermediate exogenous [NaCl] and

https://doi.org/10.1021/acs.macromol.1c00703
Macromolecules 2021, 54, 6878−6890

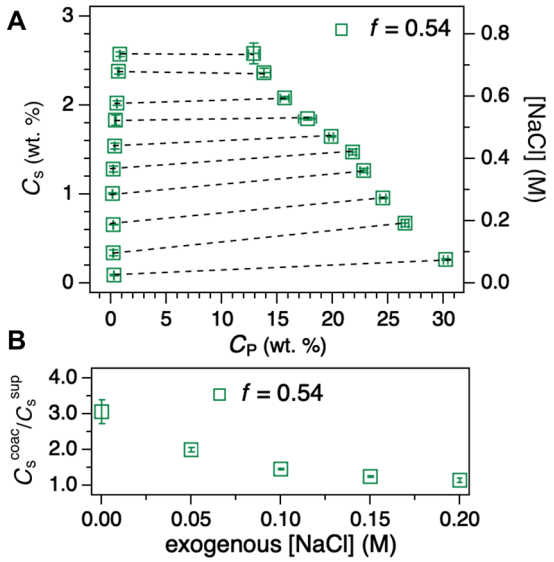

Figure 5. Salt partitioning between coacervate and supernatant phases for poly(Am_{ox}-*stat*-EO)/poly(Sulf-*stat*-EO) with $f = 0.54$. (A) Binodal phase diagram with tie lines. (B) Salt partitioning coefficient (C_s^{coac}/C_s^{sup}) vs exogenous [NaCl]. Error bars indicate the standard deviation between three separate measurements.

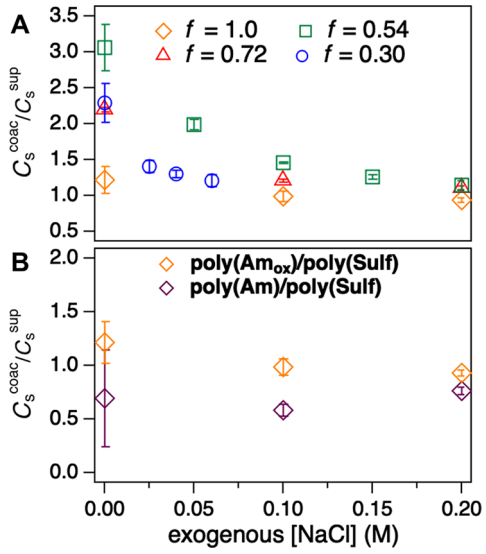

Figure 6. Salt partitioning coefficient vs exogenous [NaCl] as a function of (A) charge fraction for the oxidized series and (B) polarity of the polycation. Error bars indicate the standard deviation between three separate measurements.

level off at high [NaCl]. Positive tie line slopes indicate preferential partitioning of NaCl into the coacervate over the supernatant phase. The salt partitioning can be alternatively visualized by plotting a salt partitioning coefficient—the ratio of salt concentration in the coacervate phase (C_s^{coac}) to that in the supernatant phase (C_s^{sup})—against exogenous [NaCl] (Figure 5B). Values of $C_s^{coac}/C_s^{sup} > 1$ indicate a preference of NaCl for the coacervate phase whereas $C_s^{coac}/C_s^{sup} < 1$ specifies a preference of NaCl for the supernatant phase. As can be seen in Figure 5B, with increasing exogenous [NaCl], C_s^{coac}/C_s^{sup} approaches unity as the coacervate and supernatant phase become less distinguishable.

Similarly plotting C_s^{coac}/C_s^{sup} vs exogenous [NaCl] for all charge fractions reveals that salt partitions preferentially into the complex phase in all cases at low exogenous [NaCl] (Figure 6A and Figure S15). It appears that the salt partitioning coefficient C_s^{coac}/C_s^{sup} increases with decreasing f, although this trend reverses for $f = 0.30$. Interestingly, we found that polycation oxidation significantly impacts C_s^{coac}/C_s^{sup} (Figure 6B). Upon comparison of salt partitioning for poly(Am_{ox})/poly(Sulf) and poly(Am)/poly(Sulf), it can be seen that the relatively more hydrophobic coacervate formed from poly(Am)/poly(Sulf) partitions less salt than its corresponding supernatant phase, whereas the opposite is observed for the more polar poly(Am_{ox})/poly(Sulf).

SIMULATION RESULTS

Effect of *f* on Binodal Phase Behavior. As shown by the experimental binodals in Figure 4, a majority of (co)PEs are accumulated in the coacervate phase, serving to validate the assumption of a (co)PE-free supernatant adopted in simulations. Simulation binodals shown in Figure 7 have the same shapes and exhibit the same trends as those measured experimentally. Despite the difference in the interactions between salt ions and monomers, for both cases, the two-phase envelope narrows with increasing salt concentration. The two sets of binodal curves show a reduction of the two-phase region and a decrease of $C_{s,cr}$ with decreasing f, which agrees with experiments and is consistent with physical expectations. For salt-free coacervates, the simulation results also reveal that with decreasing f the density decrease is larger in the range of low f than in the range of high f values: The density drop from $f = 0.54$ to $f = 0.30$ is larger than that from $f = 1.0$ to $f = 0.54$. A detailed analysis of coacervate density dependence on f can be found in the Discussion section and Figure 9B.

Salt Partitioning. Figures 7A and 7B show simulation binodals for indifferent and more attractive interactions between salt and polymer, respectively. The corresponding salt partitioning coefficients are plotted against the average salt concentration in Figure 8. The average salt concentration in simulations was obtained as the ratio between the total number of salt ions in the two phases and the combined volume of the two phases. In Figure 8A, all beads experience the same excluded volume interactions, $\epsilon_{LJ} = 0.314k_BT$, and the salt partitioning coefficients C_s^{coac}/C_s^{sup} are below unity for all f values, indicating that salt ions prefer the supernatant phase. This result is in line with our experimental data for coacervates of poly(Am)/poly(Sulf) where polycations were not oxidized as well as earlier experimental findings for polypeptide PLK/PLE coacervates,[27] simulations,[27,67] and PRISM theory predictions.[75]

In addition, the salt partitioning difference between the two phases disappears; that is, C_s^{coac}/C_s^{sup} approaches unity with decreasing f and/or increasing salt concentration as the difference between the two phases diminishes. However, just by modifying the excluded volume interactions between salt ions and polymers to make salt ions more attractive to polymer beads and setting the corresponding $\epsilon_{LJ} = 0.471k_BT$, the salt partitioning can be completely changed. As shown in Figure 8B, in this case, the salt partition coefficients are above unity for all f values at low salt concentration and monotonically decrease to unity as salt concentration increases. This salt partitioning behavior agrees well with our experimental observations for poly(Am_{ox})/poly(Sulf) solutions (see Figure 6A), where salt ions preferentially partition into the coacervate phase. Similar to the former case, the salt partition difference

https://doi.org/10.1021/acs.macromol.1c00703
Macromolecules 2021, 54, 6878−6890

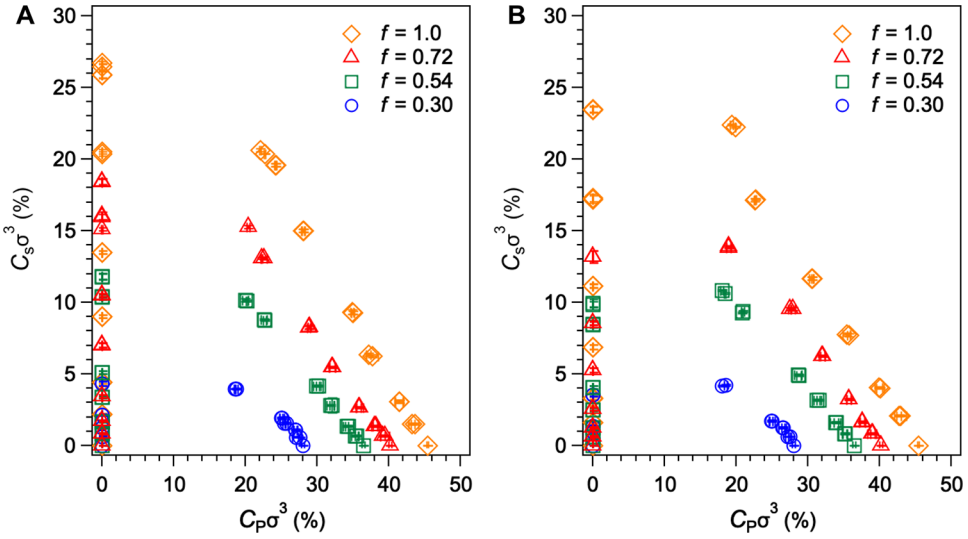

Figure 7. Binodal phase diagrams for PECs with $f = 0.30-1.0$ obtained from Gibbs ensemble simulation. (A) All beads have same LJ interactions, $\epsilon_{LJ} = 0.314k_BT$. (B) Salt−salt and monomer−monomer interactions are unchanged, $\epsilon_{LJ} = 0.314k_BT$, while for salt−monomer interactions $\epsilon_{LJ} = 0.471k_BT$ to provide stronger attractions between salt and polymer. Error bars indicate the standard deviation from the block average.

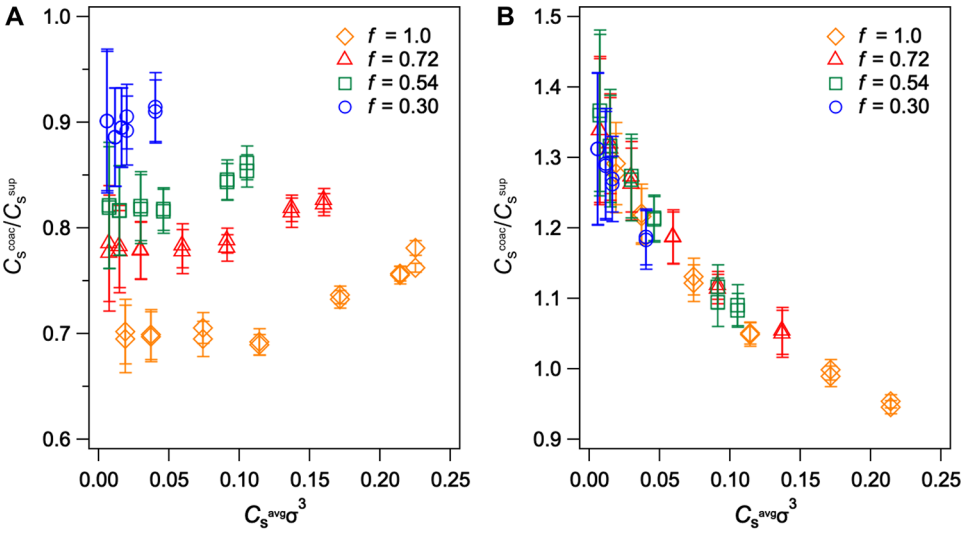

Figure 8. Salt partitioning coefficient vs average salt concentration. (A) All beads have the same LJ interactions. (B) Salt−monomer interactions are stronger than salt−salt and monomer−monomer interactions. Error bars indicate the standard deviation.

diminishes as salt concentration increases. We note that irrespective of the preferential salt partitioning to the coacervate or the supernatant at low salt concentrations, the salt partitioning coefficient C_s^{coac}/C_s^{sup} always approaches unity (decreasing or increasing, respectively) as salt is added (cf. Figures 8A and 8B). For increasing concentration of exogenous salt, the coacervate density drops, and the effect of (both Coulomb and non-Coulomb) polymer−salt interactions, which are the driving force for the uneven salt distribution between the coexisting phases, gradually weakens. A similar $C_s^{coac}/C_s^{sup} \rightarrow 1$ behavior in the high-salt regime has been also reported in ref 27.

Our simulations help rationalize the experimental results of Figure 7B and reveal that the salt partitioning between coacervate and supernatant phase is nonuniversal but instead depends strongly on the details of polymer chemistry. One can attribute the higher C_s^{coac}/C_s^{sup} for poly(Am_{ox})/poly(Sulf) coacervates as compared to poly(Am)/poly(Sulf) analogues to the better solvation of salt ions, which is itself due to the higher content of polar oxygen atoms (namely, sulfoxide and sulfonium oxygens; see Scheme 1) in the structure of the oxidized polycations. In simulations, tuning ϵ_{LJ} for polymer−salt interactions takes into account these chemistry-specific effects that are usually neglected in theoretical treatments[75,76] aimed at describing coacervate/supernatant salt partitioning.

We finally note that the nonmonotonous dependence of C_s^{coac}/C_s^{sup} on f observed in the experiments (see Figure 6A) is not reproduced in simulations where the salt partitioning coefficient is found to be almost independent of f, as seen in Figure 8B. One of the possible reasons for this discrepancy is the different solvation of Na^+ salt ions by ionic and neutral monomers, which is neglected in simulations where, for simplicity, an identical potential for interactions between salt ions and any monomer units is adopted.

https://doi.org/10.1021/acs.macromol.1c00703
Macromolecules 2021, 54, 6878−6890

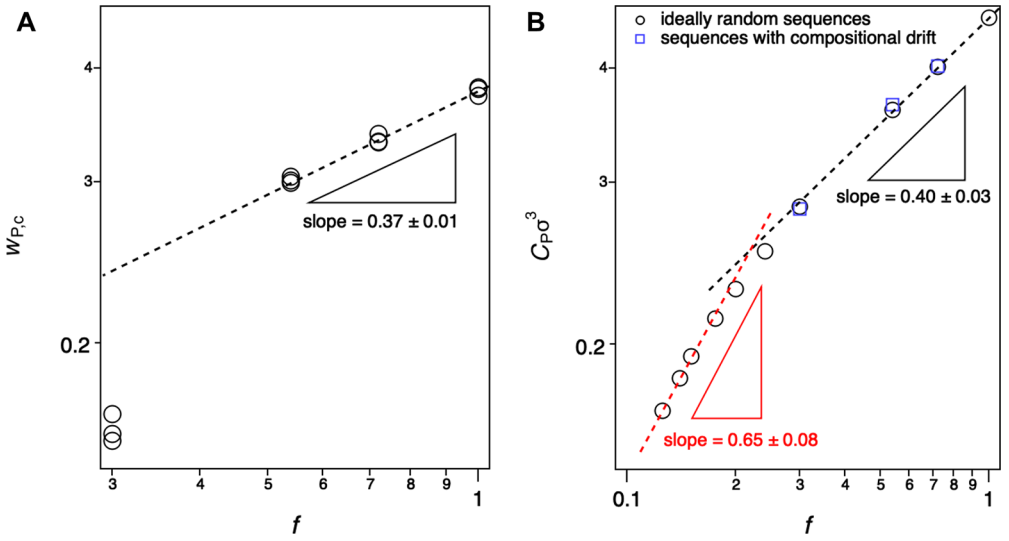

Figure 9. (A) Experimental relationship between weight fraction of (co)PE in the coacervate phase ($w_{P,c}$) at 0 M exogenous NaCl and f. (B) Coacervate density as a function of f as determined by MD simulations using chains with ideally random sequences or sequences adjusted for compositional drift and $Đ$ (experimental sequences). The slopes reported were obtained by fitting the ideally random sequences in the ranges of $0.125 \leq f \leq 0.20$ and both ideally random and experimental sequences for $0.54 \leq f \leq 1.0$.

DISCUSSION

Comparison of Theoretical Scaling Laws, MD Simulations, and Experiments. One of the motivations for this work was to access weakly charged PECs and provide a quantitative assessment of analytical scaling laws by comparing to experiments and simulations.[47−50] Within the weakly charged regime, $f \ll 1$, the density of the salt-free coacervate in a theta solvent is predicted to scale with the charge fraction as

$$\phi \simeq (uf^2)^{1/3} \tag{1}$$

where u is the dimensionless Bjerrum length $u = l_B/a = e^2/\epsilon a k_B T$ with a representing the statistical segment length and ϵ representing the dielectric constant of the solvent. For athermal solvent, this law reads $\phi \simeq (uf^2)^{(3\nu-1)/(2-\nu)} \simeq (uf^2)^{0.54}$, where $\nu = 0.588$ has been used.[48,49,65,77] The solvent quality for our chains is not currently known, but small-angle neutron studies are underway which provide insights into the structure of PECs and the chain statistics within electrostatic blobs (i.e., solvent quality). TGA of coacervates prepared at 0 M exogenous NaCl reveals a weak dependence of coacervate density—or, more accurately, PE weight fraction ($w_{P,c}$)—on charge fraction given by $w_{P,c} \sim f^{0.37\pm0.01}$ (Figure 9A). Complementary MD simulations for theta solvent conditions yield $\phi \sim f^{0.65\pm0.08}$ for $0.1 \leq f \leq 0.25$ and $\phi \sim f^{0.40\pm0.03}$ for $f \geq 0.25$ (Figure 9B). The former result is in good agreement with the scaling prediction of $\phi \sim f^{0.67}$. As anticipated, the latter deviates from scaling analysis due to lower coacervate compressibility at high densities: For theta solvent, scaling takes into account only three-body interactions,[47−50] whereas higher terms in the virial expansion become non-negligible at high ϕ. Similar deviations from the scaling predictions to the lower slopes for the $\phi(f^2)$ dependence, 0.41 ± 0.02 vs theoretical 0.54, have been recently reported for athermal solvent.[65]

The apparent slope of the experimental dependence of coacervate density on f between $0.54 < f < 1.0$ is within error of that calculated in MD simulations. A dramatic decrease in coacervate density is observed between $0.30 < f < 0.54$, but more experimental points corresponding to lower f values are required to facilitate a rigorous comparison with scaling laws. We note that decreasing f would require synthesizing longer copolyelectrolytes. For $N \approx 200$, the lowest content of ionic monomers providing phase separation is $f = 0.30$, whereas at $f = 0.10$ the solution is homogeneous even in the absence of salt. One can estimate which f values become available for longer coPEs using a simple scaling argument: an equal number of electrostatic blobs per polyion should result in similar phase behavior across different f and N values. In theta solvent, each blob consists of $g \simeq (uf^2)^{-2/3}$ monomers[47−50] and each polyelectrolyte contains $N/g \sim Nf^{4/3}$ electrostatic blobs. Assuming $N_2 = 1000$ and solving $N_1 f_1^{4/3} = N_2 f_2^{4/3}$ with $N_1 = 200$ and $f_1 = 0.30$, one can conclude that complex coacervation of longer chains is expected for $f \geq f_2 = 0.09$. Similarly, by using $f_1 = 0.10$, one obtains $f_2 = 0.03$. This suggests that for $N_2 = 1000$ coacervation will not take place for $f \leq f_2 = 0.03$. We are currently in the process of preparing chains with $N_2 = 1000$ and $0.10 \leq f \leq 0.25$ to access the range of parameters where scaling laws for coacervate densities can be rigorously and systematically corroborated.

Quantitative Comparison with Previous Coacervate Composition Data. Previously reported results by Laaser et al. can be similarly analyzed to provide a comparison to our data.[51] However, two aspects must be noted: (1) TGA data were only reported for coacervates of $f = 0.64-1.00$ prepared at 0.2 M KCl, and (2) the corresponding coacervate phases appeared to contain inhomogeneities as they were turbid (shown in photos in the authors' Supporting Information). Plotting $w_{P,c}$ vs f, apparent slopes of $w_{P,c} \sim f^{1.26}$ and $w_{P,c} \sim f^{1.41}$ are obtained for the authors' hydrophilic and hydrophobic series, respectively. This is in stark contrast to the weak dependence of coacervate density on f we observed over a comparable range of charge densities by both experiment and simulations. However, as previously mentioned, the deviations between the authors' and our system present significant challenges to a meaningful comparison of our data.

Microscopic Specificity of Interactions. Our data facilitate an evaluation of salt partitioning as a function of f

https://doi.org/10.1021/acs.macromol.1c00703
Macromolecules 2021, 54, 6878−6890

as well as of PE polarity and solvation ability. Experimentally, a preference for salt partitioning into the coacervate phase was observed at lower f values (Figure 6A) although that trend appears to reverse for $f = 0.30$. The trend observed between $f = 0.54$ and 1.0 was reproduced in simulation results (Figure 8A) and is in line with theory, which reasons that at low PEC density the finite size effect of salt ions is weak and is therefore negligible in the regime of low C_s.[48] The impact of polyelectrolyte polarity and solvation ability on salt partitioning is revealed in Figure 6B. Complexes formed from fully charged polyanions and polycations—the latter pre- and postoxidation—demonstrate the importance of the chemistry of the constituent PEs, indicating that salt partitioning is not universal. Simulation results shown in Figure 8 corroborate that this effect is attributed to the chemistry-specific interactions between salt ions and polymer. The complexes reported here feature electron-rich ether and sulfoxide/sulfonium oxygens in the polymer structures which are well-hydrated and capable of chelating Lewis acids, such as sodium ions. Hence, we attribute our observations to the combined effects of enhanced PE polarity and solvation ability. Interestingly, the same observation can be made from the data reported by Laaser and co-workers; the coacervates of the hydrophilic (L) series consistently contained a higher concentration of salt than their hydrophobic (B) analogues prepared at a similar charge fraction and identical exogenous [KCl], although this was not directly discussed in the main text (see the authors' Supporting Information, Table S1).[51] These findings are furthermore in line with previous reports by Schlenoff,[78] Larson,[79] and co-workers.

CONCLUSION

The work presented herein aimed to elucidate polyelectrolyte complex coacervate phase behavior across a broad range of charge densities. This was accomplished by employing polyether-based (co)polyelectrolytes, which remain water-soluble even at low charge fractions, due to the hydrophilic ethylene oxide comonomer. Charged moieties were carefully chosen to obtain equilibrium complexes for salt-free and salted complexes. Hydrophobic interactions were minimized by oxidation of the (co)polycation side chain thioethers to a mixture of polar sulfoxide and sulfonium species.

The charge density of polyelectrolytes f has been experimentally shown to govern their complex coacervation. The higher the f, the wider the two-phase envelope on the solution phase diagrams. For salt-free solutions, we found only a weak dependence of coacervate density on charge fraction for strongly charged complexes with $f \geq 0.5$ but noted a steep decline in coacervate density below this regime. A quantitative comparison of salt partitioning coefficients as a function of polycation polarity furthermore indicated that polar complexes partitioned salt ions more readily than their hydrophobic analogues. In contrast to most previous studies reporting higher salt concentration in the supernatant than in the coacervate, we observe that the opposite salt partitioning is also possible. This suggests that salt partitioning does not obey a universal rule but crucially depends on the polyelectrolyte chemistry defining their polarity and solvation ability. Our conclusions are supported by coarse-grained computer simulations demonstrating that salt distribution between coacervate and supernatant depends on short-range (non-Coulomb) polymer−salt interactions. In addition, salt partitioning coefficients were found to increase with decreasing charge fraction, albeit this trend appeared to reverse for the lowest charge fraction of $f = 0.30$.

Our findings provide deep insight into the role of polyelectrolyte charge density in complex coacervation, thereby providing valuable guidelines for rational design of coacervate-based materials for practical applications. Further investigations into the phase behavior, structure, and dynamics of very weakly charged chains ($f \leq 0.25$), which will facilitate a quantitative comparison with theoretical scaling laws,[47−50] are currently underway.

ASSOCIATED CONTENT

Supporting Information

The Supporting Information is available free of charge at https://pubs.acs.org/doi/10.1021/acs.macromol.1c00703.

Experimental details, polymer and polyelectrolyte characterization (^{1}H and ^{13}C NMR spectra, SEC traces), PEC characterization (microscopy and TGA data) (PDF)

AUTHOR INFORMATION

Corresponding Authors

Juan J. de Pablo − *Pritzker School of Molecular Engineering, University of Chicago, Chicago, Illinois 60637, United States; Argonne National Laboratory, Materials Science Division, Lemont, Illinois 60439, United States;* orcid.org/0000-0002-3526-516X; Email: depablo@uchicago.edu

Matthew V. Tirrell − *Pritzker School of Molecular Engineering, University of Chicago, Chicago, Illinois 60637, United States; Argonne National Laboratory, Materials Science Division, Lemont, Illinois 60439, United States;* orcid.org/0000-0001-6185-119X; Email: mtirrell@uchicago.edu

Authors

Angelika E. Neitzel − *Pritzker School of Molecular Engineering, University of Chicago, Chicago, Illinois 60637, United States; Argonne National Laboratory, Materials Science Division, Lemont, Illinois 60439, United States;* orcid.org/0000-0003-4691-5735

Yan N. Fang − *Pritzker School of Molecular Engineering, University of Chicago, Chicago, Illinois 60637, United States;* orcid.org/0000-0002-2399-9246

Boyuan Yu − *Pritzker School of Molecular Engineering, University of Chicago, Chicago, Illinois 60637, United States;* orcid.org/0000-0002-8200-4413

Artem M. Rumyantsev − *Pritzker School of Molecular Engineering, University of Chicago, Chicago, Illinois 60637, United States;* orcid.org/0000-0002-0339-2375

Complete contact information is available at: https://pubs.acs.org/10.1021/acs.macromol.1c00703

Author Contributions

A.E.N. and A.M.R. conceptualized the project. A.E.N. performed anionic polymerizations and all molecular characterizations. Y.N.F. and A.E.N. synthesized polyelectrolytes from neutral precursors. A.E.N. obtained bright field microscopy data. Y.N.F. performed the thermogravimetric analysis. B.Y. performed simulations under A.M.R.'s and J.J.d.P.'s guidance. M.V.T. and J.J.d.P. financed the study. All authors contributed to the data interpretation and writing of the manuscript.

Notes

The authors declare no competing financial interest.

■ ACKNOWLEDGMENTS

A.E.N. and Y.N.F. thank Dr. Siqi Meng for introducing them to the preparation and analysis of PECs. Parts of this work were performed at the Soft Matter Characterization Facility of the University of Chicago, and A.E.N. thanks Dr. Phil Griffin. Y.N.F. gratefully acknowledges the help of Dr. Jureller. Anionic polymerizations were performed at the Materials Science Division at Argonne National Laboratory where A.E.N. acknowledges Dr. Jun Mao, Dr. Wei Chen, and Dr. Qiming He. B.Y. and A.M.R. are grateful to Dr. Heyi Liang and Dr. Nicholas Jackson for helpful discussions. Financial support from the Center for Hierarchical Materials Design (CHiMaD) is gratefully acknowledged. This work made use of the shared facilities at the University of Chicago Materials Research Science and Engineering Center, supported by the National Science Foundation under Award DMR-2011854.

■ REFERENCES

(1) Veis, A. A review of the early development of the thermodynamics of the complex coacervation phase separation. *Adv. Colloid Interface Sci.* **2011**, *167*, 2−11.
(2) Srivastava, S., Tirrell, M. Polyelectrolyte Complexation. *Adv. Chem. Phys.*; John Wiley & Sons, Inc.: 2016; p 161.
(3) Sing, C. E.; Perry, S. L. Recent Progress in the Science of Complex Coacervation. *Soft Matter* **2020**, *16*, 2885−2914.
(4) Rumyantsev, A. M.; Jackson, N. E.; de Pablo, J. J. Polyelectrolyte Complex Coacervates: Recent Developments and New Frontiers. *Annu. Rev. Condens. Matter Phys.* **2021**, *12*, 155.
(5) van der Gucht, J.; Spruijt, E.; Lemmers, M.; Cohen Stuart, M. A. Polyelectrolyte Complexes: Bulk Phases and Colloidal Systems. *J. Colloid Interface Sci.* **2011**, *361*, 407−422.
(6) Wang, Q.; Schlenoff, J. B. The Polyelectrolyte Complex/Coacervate Continuum. *Macromolecules* **2014**, *47*, 3108−3116.
(7) Brangwynne, C. P.; Tompa, P.; Pappu, R. V. Polymer Physics of Intracellular Phase Transitions. *Nat. Phys.* **2015**, *11*, 899−904.
(8) Riback, J. A.; Zhu, L.; Ferrolino, M. C.; Tolbert, M.; Mitrea, D. M.; Sanders, D. W.; Wei, M.- T.; Kriwacki, R. W.; Brangwynne, C. P. Composition-dependent thermodynamics of intracellular phase separation. *Nature* **2020**, *581*, 209−214.
(9) Smith, J.; Calidas, D.; Schmidt, H.; Lu, T.; Rasoloson, D.; Seydoux, G. Spatial Patterning of P-granules by RNA-Induced Phase Separation of the Intrinsically-Disordered Protein MEG-3. *eLife* **2016**, *5*, No. e21337.
(10) Baer, A.; Horbelt, N.; Nijemeisland, M.; Garcia, S. J.; Fratzl, P.; Schmidt, S.; Mayer, G.; Harrington, M. J. Shear-induced β-crystallite unfolding in condensed phase nanodroplets promotes fiber formation in a biological adhesive. *ACS Nano* **2019**, *13*, 4992−5001.
(11) Stewart, R. J.; Ransom, T. C.; Hlady, V. Natural underwater adhesives. *J. Polym. Sci., Part B: Polym. Phys.* **2011**, *49*, 757−771.
(12) Fares, H. M.; Marras, A. E.; Ting, J. M.; Tirrell, M. V.; Keating, C. D. Impact of wet-dry cycling on the phase behavior and compartmentalization properties of complex coacervates. *Nat. Commun.* **2020**, *11*, 5423.
(13) Obermeyer, A. C.; Mills, C. E.; Dong, X.-H.; Flores, R. J.; Olsen, B. D. Complex coacervation of supercharged proteins with polyelectrolytes. *Soft Matter* **2016**, *12*, 3570−3581.
(14) Blocher, W. C.; Perry, S. L. Complex coacervate-based materials for biomedicine. *Wiley Interdiscip. Rev.: Nanomed. Nanobiotechnol.* **2017**, *9*, No. e1442.
(15) Krogstad, D. V.; Lynd, N. A.; Choi, S.-H.; Spruell, J. M.; Hawker, C. J.; Kramer, E. J.; Tirrell, M. V. Effects of Polymer and Salt Concentration on the Structure and Properties of Triblock Copolymer Coacervate Hydrogels. *Macromolecules* **2013**, *46*, 1512−1518.
(16) Srivastava, S.; Andreev, M.; Levi, A. E.; Goldfeld, D. J.; Mao, J.; Heller, W. T.; Prabhu, V. M.; de Pablo, J. J.; Tirrell, M. V. Gel Phase Formation in Dilute Triblock Copolyelectrolyte Complexes. *Nat. Commun.* **2017**, *8*, 14131.
(17) Black, K. A.; Priftis, D.; Perry, S. L.; Yip, J.; Byun, W. Y.; Tirrell, M. V. Protein Encapsulation via Polypeptide Complex Coacervation. *ACS Macro Lett.* **2014**, *3*, 1088−1091.
(18) McCall, P. M.; Srivastava, S.; Perry, S. L.; Kovar, D. R.; Gardel, M. L.; Tirrell, M. V. Partitioning and Enhanced Self-Assembly of Actin in Polypeptide Coacervates. *Biophys. J.* **2018**, *114*, 1636−1645.
(19) Zhao, Q.; An, Q. F.; Ji, Y.; Qian, J.; Gao, C. Polyelectrolyte Complex Membranes for Pervaporation, Nanofiltration and Fuel Cell Applications. *J. Membr. Sci.* **2011**, *379*, 19−45.
(20) Zhumadilova, G.; Gazizov, A.; Bimendina, L.; Kudaibergenov, S. Properties of Polyelectrolyte Complex Membranes Based on Some Weak Polyelectrolytes. *Polymer* **2001**, *42*, 2985−2989.
(21) Smitha, B.; Sridhar, S.; Khan, A. A. Polyelectrolyte Complexes of Chitosan and Poly(Acrylic Acid) As Proton Exchange Membranes for Fuel Cells. *Macromolecules* **2004**, *37*, 2233−2239.
(22) Meng, X.; Schiffman, J. D.; Perry, S. L. Electrospinning Cargo-Containing Polyelectrolyte Complex Fibers: Correlating Molecular Interactions to Complex Coacervate Phase Behavior and Fiber Formation. *Macromolecules* **2018**, *51*, 8821−8832.
(23) Meng, X.; Perry, S. L.; Schiffman, J. D. Complex Coacervation: Chemically Stable Fibers Electrospun from Aqueous Polyelectrolyte Solutions. *ACS Macro Lett.* **2017**, *6*, 505−511.
(24) Schaaf, P.; Schlenoff, J. B. Saloplastics: Processing Compact Polyelectrolyte Complexes. *Adv. Mater.* **2015**, *27*, 2420−2432.
(25) Yang, M.; Shi, J.; Schlenoff, J. B. Control of Dynamics in Polyelectrolyte Complexes by Temperature and Salt. *Macromolecules* **2019**, *52*, 1930−1941.
(26) Spruijt, E.; Westphal, A. H.; Borst, J. W.; Cohen Stuart, M. A.; van der Gucht, J. Binodal compositions of polyelectrolyte complexes. *Macromolecules* **2010**, *43*, 6476−6484.
(27) Li, L.; Srivastava, S.; Andreev, M.; Marciel, A. B.; de Pablo, J. J.; Tirrell, M. V. Phase behavior and salt partitioning in polyelectrolyte complex coacervates. *Macromolecules* **2018**, *51*, 2988−2995.
(28) Aumiller, W. M. J.; Keating, C. D. Phosphorylation-Mediated RNA/Peptide Complex Coacervation as a Model for Intracellular Liquid Organelles. *Nat. Chem.* **2016**, *8*, 129−137.
(29) Tabandeh, S.; Leon, L. Engineering Peptide-Based Polyelectrolyte Complexes with Increased Hydrophobicity. *Molecules* **2019**, *24*, 868−885.
(30) Vieregg, J. R.; Lueckheide, M.; Marciel, A. B.; Leon, L.; Bologna, A. J.; Rivera, J. R.; Tirrell, M. V. Oligonucleotide−Peptide Complexes: Phase Control by Hybridization. *J. Am. Chem. Soc.* **2018**, *140*, 1632−1638.
(31) Chang, L.-W.; Lytle, T. K.; Radhakrishna, M.; Madinya, J. J.; Vélez, J.; Sing, C. E.; Perry, S. L. Sequence and Entropy-Based Control of Complex Coacervates. *Nat. Commun.* **2017**, *8*, 1273.
(32) Lytle, T. K.; Chang, L.-W.; Markiewicz, N.; Perry, S. L.; Sing, C. E. Designing Electrostatic Interactions via Polyelectrolyte Monomer Sequence. *ACS Cent. Sci.* **2019**, *5*, 709−718.
(33) Rumyantsev, A. M.; Jackson, N. E.; Yu, B.; Ting, J. M.; Chen, W.; Tirrell, M. V.; de Pablo, J. J. Controlling Complex Coacervation via Random Polyelectrolyte Sequences. *ACS Macro Lett.* **2019**, *8*, 1296−1302.
(34) Lou, J.; Friedowitz, S.; Qin, J.; Xia, Y. Tunable Coacervation of Well-Defined Homologous Polyanions and Polycations by Local Polarity. *ACS Cent. Sci.* **2019**, *5*, 549−557.
(35) Li, L.; Rumyantsev, A. M.; Srivastava, S.; Meng, S.; de Pablo, J. J.; Tirrell, M. V. Effect of Solvent Quality on the Phase Behavior of Polyelectrolyte Complexes. *Macromolecules* **2021**, *54*, 105−114.
(36) Sadman, K.; Wang, Q.; Chen, Y.; Keshavarz, B.; Jiang, Z.; Shull, K. R. Influence of Hydrophobicity on Polyelectrolyte Complexation. *Macromolecules* **2017**, *50*, 9417−9426.
(37) Perry, S. L.; Leon, L.; Hoffmann, K. Q.; Kade, M. J.; Priftis, D.; Black, K. A.; Wong, D.; Klein, R. A.; Pierce, C. F.; Margossian, K. O.; Whitmer, J. K.; Qin, J.; de Pablo, J. J.; Tirrell, M. Chirality-Selected

https://doi.org/10.1021/acs.macromol.1c00703
Macromolecules 2021, 54, 6878−6890

Phase Behaviour in Ionic Polypeptide Complexes. *Nat. Commun.* **2015**, *6*, 6052.
(38) Johnston, B. M.; Johnston, C. W.; Letteri, R.; Lytle, T. K.; Sing, C. E.; Emrick, T.; Perry, S. L. The effect of comb architecture on complex coacervation. *Org. Biomol. Chem.* **2017**, *15*, 7630−7642.
(39) Yang, M.; Digby, Z.; Schlenoff, J. B. Precision Doping of Polyelectrolyte Complexes: Insight on the Role of Ions. *Macromolecules* **2020**, *53*, 5465−5474.
(40) Syed, V. M.; Srivastava, S. Time-Ionic Strength Superposition: A Unified Description of Chain Relaxation Dynamics in Polyelectrolyte Complexes. *ACS Macro Lett.* **2020**, *9*, 1067−1073.
(41) Meng, S.; Liu, Y.; Yeo, J.; Ting, J. M.; Tirrell, M. V. Effect of mixed solvents on polyelectrolyte complexes with salt. *Colloid Polym. Sci.* **2020**, *298*, 887−894.
(42) Weinbreck, F.; de Vries, R.; Schrooyen, P.; de Kruif, C. G. Complex Coacervation of Whey Proteins and Gum Arabic. *Biomacromolecules* **2003**, *4*, 293−303.
(43) Ali, S. A.; Bleuel, M.; Prabhu, V. M. Lower Critical Solution Temperature in Polyelectrolyte Complex Coacervates. *ACS Macro Lett.* **2019**, *8*, 289−293.
(44) Bungenberg-De Jong, H.; Kruyt, H. *Proc. Sect. Sci., K. Ned. Akad. Wetenschappen* **1929**, *32*, 849−856.
(45) Overbeek, J. T. G.; Voorn, M. J. Phase Separation in Polyelectrolyte Solutions. Theory of Complex Coacervation. *J. Cell. Comp. Physiol.* **1957**, *49* (S1), 7−26.
(46) Neitzel, A. E.; De Hoe, G. X.; Tirrell, M. V. Expanding the Structural Diversity of Polyelectrolyte Complexes and Polyzwitterions. *Curr. Opin. Solid State Mater. Sci.* **2021**, *25*, 100897.
(47) Shusharina, N. P.; Zhulina, E. B.; Dobrynin, A. V.; Rubinstein, M. Scaling Theory of Diblock Polyampholyte Solutions. *Macromolecules* **2005**, *38*, 8870−8881.
(48) Rumyantsev, A. M.; Zhulina, E. B.; Borisov, O. V. Complex Coacervate of Weakly Charged Polyelectrolytes: Diagram of States. *Macromolecules* **2018**, *51*, 3788−3801.
(49) Rubinstein, M.; Liao, Q.; Panyukov, S. Structure of Liquid Coacervates Formed by Oppositely Charged Polyelectrolytes. *Macromolecules* **2018**, *51*, 9572−9588.
(50) Danielsen, S. P. O.; Panyukov, S.; Rubinstein, M. Ion Pairing and the Structure of Gel Coacervates. *Macromolecules* **2020**, *53*, 9420−9422.
(51) Huang, J.; Morin, F. J.; Laaser, J. E. Charge-Density-Dominated Phase Behavior and Viscoelasticity of Polyelectrolyte Complex Coacervates. *Macromolecules* **2019**, *52*, 4957−4967.
(52) Lee, B. F.; Wolffs, M.; Delaney, K. T.; Sprafke, J. K.; Leibfarth, F. A.; Hawker, C. J.; Lynd, N. A. Reactivity Ratios and Mechanistic Insight for Anionic Ring-Opening Copolymerization of Epoxides. *Macromolecules* **2012**, *45*, 3722−3731.
(53) Kharel, A.; Lodge, T. P. Coil Dimensions of Poly(ethylene oxide) in an Ionic Liquid by Small-Angle Neutron Scattering. *Macromolecules* **2017**, *50*, 8739−8744.
(54) Kremer, K.; Grest, G. S. Dynamics of entangled linear polymer melts: A molecular dynamics simulation. *J. Chem. Phys.* **1990**, *92*, 5057−5086.
(55) Plimpton, S.; Hendrickson, B. Parallel Molecular Dynamics Algorithms for Simulation of Molecular Systems. In *Parallel Computing in Computational Chemistry*; ACS Symposium Series; American Chemical Society: 1995; Vol. *592*, pp 114−132.
(56) Graessley, W. W.; Hayward, R. C.; Grest, G. S. Excluded-volume effects in polymer solutions. 2. Comparison of experimental results with numerical simulation data. *Macromolecules* **1999**, *32*, 3510−3517.
(57) Grzetic, D. J.; Delaney, K. T.; Fredrickson, G. H. The Effective χ Parameter in Polarizable Polymeric Systems: One-Loop Perturbation Theory and Field-Theoretic Simulations. *J. Chem. Phys.* **2018**, *148*, 204903.
(58) Kong, X.; Hou, K. J.-Y.; Qin, J. Weakening of Solvation-Induced Ordering by Composition Fluctuation in Salt-Doped Block Polymers. *ACS Macro Lett.* **2021**, *10*, 545−550.
(59) Shen, K.-H.; Fan, M.; Hall, L. M. Molecular Dynamics Simulations of Ion-Containing Polymers Using Generic Coarse-Grained Models. *Macromolecules* **2021**, *54*, 2031−2052.
(60) Gavrilov, A. A. Dissipative Particle Dynamics for Systems with Polar Species: Interactions in Dielectric Media. *J. Chem. Phys.* **2020**, *152*, 164101.
(61) Mintis, D. G.; Mavrantzas, V. G. Phase Boundary and Salt Partitioning in Coacervate Complexes Formed between Poly(Acrylic Acid) and Poly(N,N-Dimethylaminoethyl Methacrylate) from Detailed Atomistic Simulations Combined with Free Energy Perturbation and Thermodynamic Integration Calculations. *Macromolecules* **2020**, *53*, 7618−7634.
(62) Fredrickson, G. H.; Milner, S. T.; Leibler, L. Multicritical Phenomena and Microphase Ordering in Random Block Copolymer Melts. *Macromolecules* **1992**, *25*, 6341−6354.
(63) Smith, A. A.; Hall, A.; Wu, V.; Xu, T. Practical prediction of heteropolymer composition and drift. *ACS Macro Lett.* **2019**, *8*, 36−40.
(64) https://github.com/vince-wu/CompositionalDrift.
(65) Yu, B.; Rauscher, P. M.; Jackson, N. E.; Rumyantsev, A. M.; de Pablo, J. J. Crossover from Rouse to Reptation Dynamics in Salt-Free Polyelectrolyte Complex Coacervates. *ACS Macro Lett.* **2020**, *9*, 1318−1324.
(66) Gartner III, T. E.; Epps III, T. H.; Jayaraman, A. Leveraging Gibbs Ensemble Molecular Dynamics and Hybrid Monte Carlo/Molecular Dynamics for Efficient Study of Phase Equilibria. *J. Chem. Theory Comput.* **2016**, *12*, 5501−5510.
(67) Radhakrishna, M.; Basu, K.; Liu, Y.; Shamsi, R.; Perry, S. L.; Sing, C. E. Molecular connectivity and correlation effects on polymer coacervation. *Macromolecules* **2017**, *50*, 3030−3037.
(68) Panagiotopoulos, A. Z.; Quirke, N.; Stapleton, M.; Tildesley, D. Phase equilibria by simulation in the Gibbs ensemble: Alternative derivation, generalization and application to mixture and membrane equilibria. *Mol. Phys.* **1988**, *63*, 527−545.
(69) Plimpton, S. Fast Parallel Algorithms for Short-Range Molecular Dynamics. *J. Comput. Phys.* **1995**, *117*, 1−19.
(70) Lodge, T. P.; Hiemenz, P. C. *Polymer Chemistry*, 2nd ed.; CRC Press: Boca Raton, FL, 2007.
(71) Lee, B. F.; Kade, M. J.; Chute, J. A.; Gupta, N.; Campos, L. M.; Fredrickson, G. H.; Kramer, E. J.; Lynd, N. A.; Hawker, C. J. Poly(allylGlycidyl Ether)-A Versatile and Functional Polyether Platform. *J. Polym. Sci., Part A: Polym. Chem.* **2011**, *49*, 4498−4504.
(72) Zydziak, N.; Haseeb Iqbal, M.; Chaumont, A.; Combes, A.; Wasielewski, E.; Legros, M.; Jierry, L.; Lavalle, P.; Boulmedais, F.; Chan-Seng, D. Unexpected aqueous UCST behavior of a cationic comb polymer with pentaarginine side chains. *Eur. Polym. J.* **2020**, *125*, 109528.
(73) Shih, O.; England, A. H.; Dallinger, G. C.; Smith, J. W.; Duffey, K. C.; Cohen, R. C.; Prendergast, D.; Saykally, R. J. Cation-Cation Contact Pairing in Water: Guanidinium. *J. Chem. Phys.* **2013**, *139*, 035104.
(74) Li, L.; Srivastava, S.; Meng, S.; Ting, J. M.; Tirrell, M. V. Effects of Non-Electrostatic Intermolecular Interactions on the Phase Behavior of pH-sensitive Polyelectrolyte Complexes. *Macromolecules* **2020**, *53*, 7835−7844.
(75) Perry, S. L.; Sing, C. E. PRISM-Based Theory of Complex Coacervation: Excluded Volume versus Chain Correlation. *Macromolecules* **2015**, *48*, 5040−5053.
(76) Zhang, P.; Shen, K.; Alsaifi, N. M.; Wang, Z.-G. Salt Partitioning in Complex Coacervation of Symmetric Polyelectrolytes. *Macromolecules* **2018**, *51* (15), 5586−5593.
(77) Wang, Z.; Rubinstein, M. Regimes of Conformational Transitions of a Diblock Polyampholyte. *Macromolecules* **2006**, *39*, 5897−5912.
(78) Schlenoff, J. B.; Yang, M.; Digby, Z. A.; Wang, Q. Ion Content of Polyelectrolyte Complex Coacervates and the Donnan Equilibrium. *Macromolecules* **2019**, *52*, 9149−9159.

https://doi.org/10.1021/acs.macromol.1c00703
Macromolecules 2021, 54, 6878−6890

(79) Ghasemi, M.; Friedowitz, S.; Larson, R. G. Analysis of Partitioning of Salt through Doping of Polyelectrolyte Complex Coacervates. *Macromolecules* **2020**, *53*, 6928−6945.

https://doi.org/10.1021/acs.macromol.1c00703
Macromolecules 2021, 54, 6878−6890